

A model study of enhanced oil recovery by flooding with aqueous surfactant solution and comparison with theory.

Paul D.I. Fletcher*, Luke D. Savory and Freya Woods

Surfactant & Colloid Group, Department of Chemistry,

University of Hull, Hull. HU6 7RX. U.K.

Andrew Clarke and Andrew M. Howe

Schlumberger Gould Research, High Cross, Madingley Road, Cambridge CB3 0EL

*Author for correspondence: Prof. P.D.I. Fletcher

E mail: P.D.Fletcher@hull.ac.uk

Abstract

With the aim of elucidating the details of enhanced oil recovery by surfactant solution flooding, we have determined the detailed behaviour of model systems consisting of a packed column of calcium carbonate particles as the porous rock, n-decane as the trapped oil and aqueous solutions of the anionic surfactant sodium bis-2-ethylhexyl sulfosuccinate (AOT). The AOT concentration was varied from zero to above the critical aggregation concentration (cac). The salt content of the aqueous solutions was varied to give systems of widely different, post-cac oil-water interfacial tensions. The systems were characterised in detail by measuring the permeability behaviour of the packed columns, the adsorption isotherms of AOT from the water to the oil-water interface and to the water-calcium carbonate interface and oil-water-calcium carbonate contact angles. Measurements of the %oil recovery by pumping surfactant solutions into calcium carbonate packed columns initially filled with oil were analysed in terms of the characterisation results. We show that the measured contact angles as a function of AOT concentration are in reasonable

agreement with those calculated from values of the surface energy of the calcium carbonate-air surface plus the measured adsorption isotherms. Surfactant adsorption onto the calcium carbonate-water interface causes depletion of its aqueous phase concentration and we derive equations which enable the concentration of non-adsorbed surfactant within the packed column to be estimated from measured parameters. The %oil recovery as a function of the surfactant concentration is determined solely by the oil-water-calcium carbonate contact angle for non-adsorbed surfactant concentrations less than the cac. For surfactant concentrations greater than the cac, additional oil removal occurs by a combination of solubilisation and emulsification plus oil mobilisation due to the low oil-water interfacial tension and a pumping pressure increase.

Introduction

Primary and secondary oil recovery processes generally leaves of the order of 50% of the total oil underground where a large proportion is trapped within the porous reservoir rock by capillary forces but other effects such as flow bypassing due to heterogeneous permeability can also be important. One of the tertiary recovery processes used to release oil trapped by capillary forces is enhanced oil recovery (EOR) by injection of aqueous surfactant solution into the partially depleted reservoir. Because of its obvious economic importance, there is an extensive literature on the inter-related aspects of this complex process; including general reviews and measurements of the EOR performance of different surfactant systems¹⁻⁹, studies of how exposure of the porous network to crude oil and water leads to complex “mixed wettabilities” in which the pores are partially wetted by both oil and water and how surfactant addition alters the wettability state of the reservoir¹⁰⁻¹⁴, visualisation of the complex, multiphase flow¹⁵⁻¹⁸ and modelling of how the oil recovery depends on the pore network structure, wettability state, relative permeabilities to oil and water, flow rates and other conditions¹⁹⁻²⁶. However, this literature does not contain clear, systematic information on how the rock/oil/water contact angle varies with surfactant concentration and how this relates to surfactant adsorption at the various surfaces present, how surfactant adsorption causes its depletion

in the EOR aqueous phase, and how these factors relate to the fraction of oil recovered. To address these issues, we have investigated how aqueous solutions of the anionic surfactant sodium bis(2-ethylhexyl) sulfosuccinate (AOT) removes *n*-decane oil from packed columns containing calcium carbonate calcite particles.

This paper is organised as follows. Following the experimental section, the liquid flow properties of the calcite particle packed columns are summarised. Next, we report measurements of the adsorption isotherm of AOT to the calcite-water interface, water-decane tensions and water-decane-calcite contact angles as a function of surfactant concentration and show how the contact angles can be derived from considerations of the surface energies and adsorption. Then, we show how the %oil recovery varies with surfactant concentration for selected aqueous phase salt concentrations which control the equilibrium microemulsion phase behaviour and whether or not the oil-water tension reaches ultralow values. Prior to interpretation of the %oil recovery results, it is important to note that measurements of adsorption, oil-water interfacial tension and contact angle relate to the concentration of *non-adsorbed* surfactant whereas %oil recovery relates to the *initial* surfactant concentration which is depleted due to adsorption. Hence, we show how surfactant adsorption measurements can be used to estimate the concentration of *non-adsorbed* surfactant present within the packed columns during EOR. Finally, we show how the measured %oil recovery variation with surfactant concentration is consistent with a model based on the hypothesis that the residual oil is trapped in the form of liquid bridges between contacting calcite particles.

It is worth noting here that, in addition to being relevant to EOR, considerations of the amount of fluid retained when a particle bed is flooded with a second fluid are also important in the prediction of so-called “liquid holdup” in distillation columns and catalyst particle bed reactors²⁷⁻²⁹.

Experimental

Materials. Three calcium carbonate powders of different mean particle sizes were obtained from Minelco UK as part of their Fordacal product range which consists of natural ground calcium

carbonate of different particle size distributions. Figure S1 shows SEM images of the three powders and Table 1 summarises their average particle radii from SEM images and sieve analysis data supplied by Minelco (Figure S3) and specific surface areas, porosities and average pore diameters obtained from BET analysis of nitrogen adsorption isotherms. The SEM images show the particles are irregularly-shaped and polydisperse. X-ray diffraction measurements confirmed that the powders all consist virtually exclusively of the calcite polymorph of calcium carbonate. The BET nitrogen adsorption/desorption isotherms showed no significant hysteresis in the case of FC10 but significant hysteresis was observed for FC30 and FC200. The total specific surface areas measured using BET are 10-400 fold larger than those estimated for monodisperse, non-porous spheres of the corresponding mean particle radii ($0.8 \text{ m}^2 \text{ g}^{-1}$ for FC10, $0.2 \text{ m}^2 \text{ g}^{-1}$ for FC30 and $0.05 \text{ m}^2 \text{ g}^{-1}$ for FC200) and hence are dominated by particle internal pore surface areas. As seen in Table 1, the particle internal pores have volume fractions from 0.08 to 0.04 with average diameters from 110 to 26 nm.

Calcite crystals for contact angle measurements were obtained from John Brommeland (www.brommeland.com) in Norway. They were cut to size and the top surface was polished using abrasive paper with a particle size of 4.5 microns.

Water was purified by passing through an Elgastat Prima reverse osmosis unit followed by a Millipore Milli-Q reagent water system. Its resistivity was $16 \text{ M}\Omega \text{ cm}$ and its surface tension was 71.9 mN m^{-1} at 25°C . The anionic surfactant sodium bis(2-ethylhexyl) sulfosuccinate (AOT, Sigma-Aldrich, 98%) was used as-received. Some samples of *n*-decane (Sigma, >99%) were columned over basic alumina (Merck) to remove any polar impurities prior to use. However, it was found that using either columned or as-received *n*-decane made no significant difference to either the oil-water tension or %oil recovery measurements. Most measurements were made using as-received *n*-decane. The salts NaCl (Fisher, 99.9%) and Na_2CO_3 (Fisher, 99%) were used as received. Reagents used in the titrations to determine AOT concentrations, Hyamine 1622 (Fluka, 98%),

dimidium bromide (Sigma, 95%), disulfine blue (Sigma, 50% dye content) and chloroform (Fisher, analytical reagent grade) were used as received.

Methods.

Scanning electron microscopy (SEM). SEM images of the calcite powders were obtained using a Zeiss EVO60 electron microscope. Samples were sputter coated with a 2 nm thick Au/Pd (Au 82%, Pd 18%) film prior to imaging. SEM images were analysed to estimate the mean particle diameters (taken to be the average of longest and shortest dimensions and averaged over >20 individual particles) using Image J software.

Nitrogen adsorption isotherms and analysis. Nitrogen adsorption isotherms onto the calcite powders at the boiling temperature of liquid nitrogen were measured using a Micromeritics TriStar 3000 instrument. The results were analysed using the method described in detail by Barret , Joyner and Halenda³⁰.

Flow properties and oil removal from packed columns containing calcite particles. The experimental setup used to investigate the flow properties and oil removal for calcite powder packed columns is shown in Figure 1. The column is a modular semi-preparative HPLC stainless steel cylindrical column (Kinesis, UK) with an internal diameter of 10 mm and an internal length of 50 mm fitted with PEEK connectors for flow tubing. The following procedure is used to pack the column with calcite powder. One end of the column is first sealed with a frit (mean pore diameter 2 μm , thickness 1 mm supplied by Kinesis) and end connector. The calcite powder is then added in small aliquots and a metal rod and hammer used to pack the powder down between aliquots. When full of powder, the second frit is added and the assembly sealed with the second end connector. It is worth noting that the pore diameter of the frits is much larger than the mean pore size within the packed columns; as seen later the frits contribute only a small fraction of the overall hydrodynamic resistance of the filled column. The column is weighed before and after filling to determine the mass (and hence volume fraction) of powder in the packed column volume.

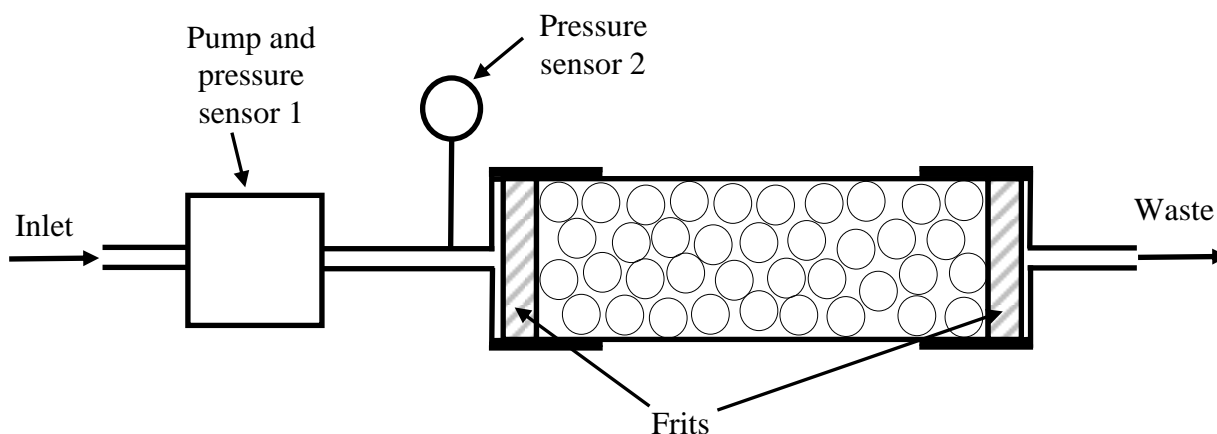


Figure 1. Schematic of the packed powder column flood setup.

Two types of experiment have been performed with the packed columns. In the first type, used to determine the flow properties of the packed columns, pure water or pure decane was flowed through the column initially containing only powder to displace air. Using measurements of the mass before and after decane filling, it was checked that the final volume fraction of trapped air was less than 0.01. The volumetric flow rate was set using the HPLC or syringe pump and the pressure drop between the pump and the column exit was monitored. The second type of experiment was used to determine the amount of oil displaced by flowing an aqueous solution into a powder packed column with decane-filled interstices. The powder packed column interstices were filled with decane using a syringe pump (WPI model sp100i) with a volumetric flow rate of $8.3 \mu\text{l min}^{-1}$ for approximately 5 pore volumes. Again, the column is weighed before and after the oil filling to determine the mass of decane initially in the packed column and to check that the column contains virtually no trapped air. The column is then attached to an HPLC pump (Jasco PU-1580 or PU-980 Intelligent HPLC Pump) and the aqueous surfactant solution pumped at a set flow rate and the total pressure drop monitored. To determine the amount of oil removed from the column, the pump is stopped, the column removed and weighed at appropriate time intervals. Since the density of decane (0.7264 g cm^{-3} at 25°C) is different from the density of the aqueous surfactant solution (approx. 1.0 g cm^{-3} , measured precisely for each aqueous phase composition), the mass of the column increases slightly as decane is displaced from the column and the measured masses can be used to derive the

percent of the original oil in place recovered (%oil recovery). From repeated measurements, we estimate the uncertainty in an individual column mass measurement to be ± 4 mg (this is larger than the uncertainty resulting from the balance owing to the requirement to disconnect the column and drying the connections prior to each weighing). Since the difference in mass of the column filled with decane and filled with water is approximately 400 mg, this uncertainty in the individual mass measurements corresponds to an uncertainty in the final value of %oil recovered of $\pm 2\%$. Solution densities required for this calculation were measured using an Anton Paar DMA 35N density meter.

Adsorption isotherms. The adsorption isotherms for AOT adsorbing from aqueous solution to the calcite powder surfaces were measured by a depletion method as follows. 20 ml of the required concentration of surfactant solution and a known mass of calcium carbonate powder were added to a 60 ml glass jar fitted with screw top lid and a magnetic stirrer bar. The pH was measured with a Jenway 3510 pH meter and adjusted as required. The samples were mounted within a thermostat bath placed on top of a Variomag Poly 15 multipoint magnetic stirrer and were equilibrated with stirring at 700 rpm for over 6 hours. Using repeat measurements with different equilibration times, 6 hours was found to be sufficient to ensure equilibrium was reached. After equilibration, the sample was centrifuged at 6000 rpm for 5 minutes using a Baird & Tatlock Mk IV Auto Bench Centrifuge to separate the calcium carbonate particles. The supernatant was titrated to determine the final AOT concentration using the surfactant titration method detailed in ref 31.

Decane-aqueous solution interfacial tensions. Decane-water interfacial tensions above 5 mN m^{-1} were measured using the static maximum pull method with a Krüss K12 instrument using a du Noüy ring. Tensions below 5 mN m^{-1} , including ultralow values, were measured using a Krüss SITE 04 spinning drop tensiometer.

Contact angles. Contact angles (static, advanced) of drops of aqueous solution on calcite crystals under decane were measured as follows. Calcite crystals were cut to a size of 9 mm x 9 mm x 9 mm, polished, cleaned with heptane, dried using compressed air and placed in a glass 10 mm path length

cuvette. The cuvette containing the crystal was filled with decane and placed in the thermostatted cell of a Krüss DSA 10 instrument. A 0.2-0.5 μl sessile drop of the aqueous solution was carefully injected on to the calcite surface, making sure to avoid any voids or cracks that occur in the crystal. To obtain reliable contact angles, it is important that the field of view size of the three phase contact line of the sessile drop is similar to or smaller than the capillary length of the oil-water interface ($= (\gamma/\Delta\rho g)^{1/2}$ where γ is the oil-water tension, $\Delta\rho$ is the density difference between the two fluid phases and g is acceleration due to gravity). Systems with an ultra-low oil-water interfacial tension consequently have a very small capillary length and thus require small drop volumes and high magnification to determine the contact angle. The horizontal microscope used here consisted of a Navitar 1-60350 zoom system equipped with a Mitutoyo M Plan Apo 5 objective lens (magnification 5X, numerical aperture 0.14, working distance 34.0 mm) and a QImaging QICam digital camera which enabled overall magnification of approximately 100X. Micrographs were taken of the static advanced sessile drop and the contact angle measured with an on-screen protractor using Iconico software (New York, Version 4.0). Contact angles were observed to reach a constant value within 1 minute or so and did not change significantly over periods of up to several hours. For Winsor III systems containing three fluid phases, small drops of the third (surfactant-rich phase) were observed to separate from the main water drop. In all cases, the contact angle measured corresponded to the calcite-(water-rich)-(decane-rich) three phase contact line.

All measurements were made at a temperature of 25°C and pH of the aqueous solutions in the range 9.0 to 10.8. For selected measurements, it was checked that changing the pH from 9.0 to 10.8 produced no significant differences.

Results and Discussion

Characterisation of the calcite particles and the flow properties of packed columns.

Table 1 summarises the average particle radii, specific surface areas and the radii and volumes of the internal pores within the calcite particles for the three calcite powders. As described

in the ESI, the permeabilities of the powder packed columns were measured and used to derive the effective average pore radii corresponding to the interstices between the particles.

Powder	Average particle radius / μm	specific surface area / $\text{m}^2 \text{g}^{-1}$	Powder particle internal pore volume fraction	Powder particle internal pore radius/nm	Packed column pore volume fraction ϕ_{pore}	Average effective pore radius (ESI Eq. 4) $r_{\text{pore}}/\mu\text{m}$
FC10	1.4	8.6	0.08	110	0.45	0.16
FC30	5.0	10	0.04	49	0.40	0.33
FC200	23	19	0.05	26	0.34	0.69

Table 1. Properties of the calcium carbonate powders used and packed columns containing the powders. The average particle radii correspond to the average of the radii at 50% of the cumulative distribution from sieving analysis and the mean radii derived from SEM images.

Adsorption of AOT at the aqueous solution-calcite interface and the aqueous solution-decane interfaces and the contact angles.

Surfactant EOR is thought to be optimal for oil/water/surfactant systems which, at equilibrium, form microemulsion phases and exhibit ultralow oil-water interfacial tensions³²⁻³⁵. The choice of AOT with decane and aqueous salt solutions for this study was driven by the fact that the equilibrium properties of these mixtures are well characterised³⁶⁻³⁷. As shown in Table 2, we have used three different salt concentration systems here and list the corresponding aqueous phase critical microemulsion concentrations ($c_{\mu\text{c}}$), equilibrium microemulsion phase type (Winsor I or III) formed in systems containing excess oil phase and the post- $c_{\mu\text{c}}$ water-decane interfacial tensions. However, it is important to note that, as in the case of surfactant EOR flooding generally, the aqueous AOT solutions used in the calcite particle packed column experiments are not pre-equilibrated with the decane phase. Aqueous solutions containing the salt concentrations shown and AOT concentrations above a critical aggregation concentration (c_{ac}) (with values generally similar to the aqueous phase $c_{\mu\text{c}}$) prior to equilibration with decane form a turbid dispersion of lamellar phase,

probably in the form of multilamellar, “onion-like” vesicles³⁸⁻³⁹. On equilibration with decane, these mixtures solubilise decane to form either oil-in-water or bicontinuous microemulsions.

[NaCl] /mM	[Na ₂ CO ₃] /mM	Aqueous phase $c_{\mu c}$ (with decane) /mM	Post- $c_{\mu c}$ water-decane interfacial tension /mN m ⁻¹	Winsor system type	Contact angle θ in the absence of surfactant/ ^o	%oil recovery in the absence of surfactant
0	10	1.0	0.33	I	123	74
40	10	0.60	0.028	I	126	77
75	10	0.55	0.0079	III	120	73

Table 2. Compositions and properties of the aqueous AOT surfactant solutions used.

It is envisaged that the removal of decane trapped within the pores of the calcite packed columns by AOT solutions of different concentrations will depend on the decane-water-calcite contact angle, the decane-water interfacial tension and the extent to which AOT is depleted from the aqueous solution by adsorption. The contact angle is determined by the balance of the decane-water, calcite-decane and calcite-water interfacial tensions which vary with [AOT] due to adsorption at the different interfaces. In this section, we show how AOT adsorbs at the different interfaces and how this leads to the observed variation of contact angle with AOT concentration.

Figure 2 shows the adsorption isotherms for AOT from aqueous solutions to the calcite-water interface. Qualitatively, it can be seen that the adsorption of AOT monomers is weak until just below the critical *aggregation* concentration of the AOT (expected to be similar to the critical *microemulsion* concentrations listed in Table 2 for the different systems). Above this point there is a highly co-operative adsorption to form adsorbed films with surface concentrations of around 2 molecules nm⁻². The iso-electric point of the calcite-water interface is approximately pH 9.5⁴⁰⁻⁴⁵ which is within the range of pH values used here (9.0 to 10.8). Hence, the driving force for AOT adsorption does not include strong electrostatic interaction but is likely to be dominated by hydrophobic interactions leading to the observed highly co-operative adsorption at AOT concentrations similar to the relevant c_{ac} . Following trials with several different theoretical

adsorption isotherms⁴⁶⁻⁴⁷, the plots of Figure 2 were fitted to a Langmuir-type isotherm modified to take account of cooperative adsorption through the parameter β (equation 1)⁴⁶.

$$[surf]_{non-adsorbed} = \frac{(\Gamma/\Gamma_{max})}{(1 - (\Gamma/\Gamma_{max})) \cdot K \cdot e^{-\beta\Gamma/\Gamma_{max}}} \quad (1)$$

where $[surf]_{non-adsorbed}$ is the equilibrium concentration of non-adsorbed surfactant, Γ is the surface concentration of adsorbed surfactant, Γ_{max} is the maximum surface concentration, K is a constant reflecting the strength of adsorption and β is the co-operativity parameter. When β is equal to zero, the isotherm reduces to the Langmuir isotherm; $\beta > 0$ corresponds to anti-co-operative adsorption and $\beta < 0$ corresponds to co-operative adsorption. For the 75 mM NaCl system, the parameters of the fit shown in Figure 2 are $\Gamma_{max} = 2.2$ molecules nm^{-2} , $K = 0.446$ mM^{-1} and $\beta = -4.0$. The adsorption isotherms of Figure 2 are similar to those seen in a previous study of AOT adsorption on calcite⁴⁸.

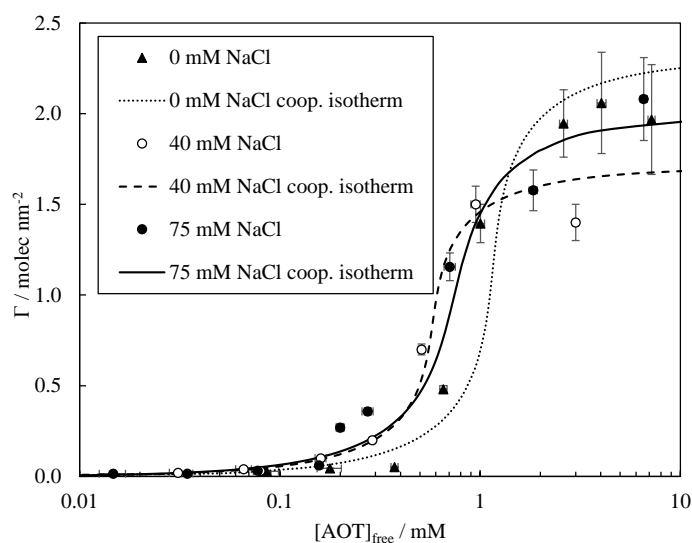


Figure 2. Adsorption isotherm for the adsorption of AOT to the calcite-aqueous solution interface from aqueous solutions at $pH\ 9.3 \pm 0.3$ and containing 10 mM Na_2CO_3 plus the NaCl concentrations indicated. The curved solid line shows the best fits to the cooperative isotherm (equation 1) with the parameters given in the text.

Figure 3 shows the variation of the decane-water tension with AOT concentration for the three different salt concentrations. Due to adsorption of AOT monomers at the water-decane

interface, the tension decreases from 42.5 mN m^{-1} (in the absence of AOT) to a value independent of AOT concentration at the $c_{\mu c}$. Above the $c_{\mu c}$ the tension is constant as the AOT in excess of the $c_{\mu c}$ forms microemulsion aggregates which do not adsorb at the water-decane interface. As summarised in Table 2, the $c_{\mu c}$ and the post- $c_{\mu c}$ interfacial tension depend on the salt concentration.

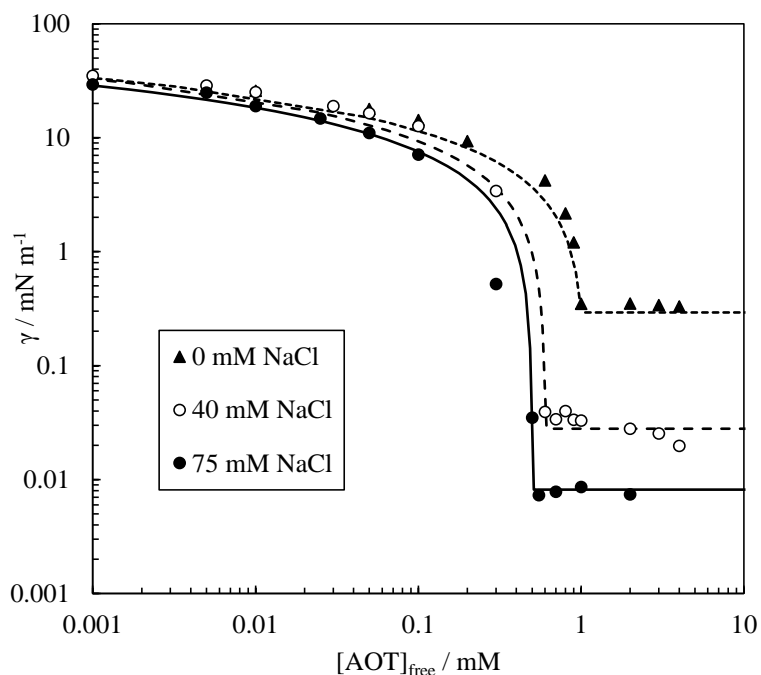


Figure 3. Variation of decane-water tension with aqueous AOT concentration at 25.0°C for solutions containing $10 \text{ mM Na}_2\text{CO}_3$ plus the NaCl concentrations indicated. The curved solid lines show the best-fits calculated as described in the text.

For the 75 mM NaCl system, the decane-water-calcite contact angle (measured through the water) is $120 \pm 10^\circ$. As seen in Figure 4, the contact angle increases slightly with increasing $[\text{AOT}]$, decreases sharply around the $c_{\mu c}$ and finally decreases slightly further before reaching a high $[\text{AOT}]$ plateau value of approximately 15° . The contact angle behaviour of the systems containing 0 and 40 mM NaCl (not shown) is qualitatively similar; the following discussion focuses on the 75 mM NaCl system.

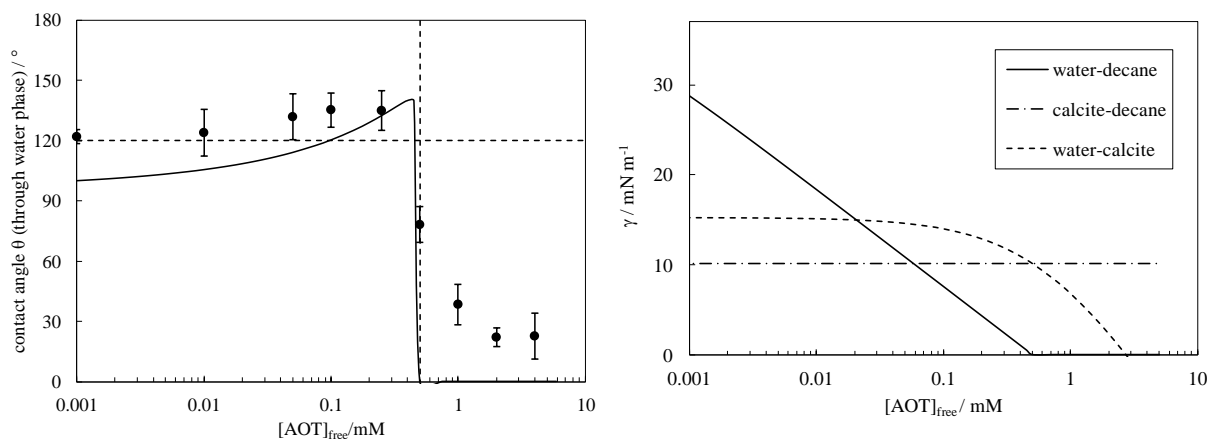


Figure 4. Left plot: Variation of decane-water-calcite contact angle (measured through the aqueous phase) with aqueous AOT concentration for solutions containing 75 mM NaCl and 10 mM Na₂CO₃. The vertical dashed line indicates the $c_{\mu c}$. The horizontal dashed lined shows the contact angle in the absence of added AOT. The solid line shows the calculated contact angle from the water-decane (measured), water-calcite (derived from the measured adsorption isotherm) and decane-calcite (invariant with $[AOT]$) tensions shown in the right hand plot.

The equilibrium calcite-water-decane contact angle is determined by the relative magnitudes of the calcite-water, decane-water and calcite-decane interfacial tensions. The three interfacial tensions in the absence of AOT can be estimated using considerations of the polar and dispersion force contributions to the excess surface energies (surface tensions) of each component. The interfacial surface energy of any substance x against air (γ_{x-air}) can be expressed as the sum of the components arising from the polar and dispersion forces (γ^p and γ^d respectively) as shown in equation 2⁴⁹.

$$\gamma_{x-air} = \gamma_{x-air}^p + \gamma_{x-air}^d \quad (2)$$

Values of γ^p and γ^d derived from tension and contact angles and other methods are available in the literature. Values (γ^p and γ^d respectively) are 50.4 and 21.5 mJ m⁻² for water⁴⁹, 0 and 23.8 mJ m⁻² for decane⁴⁹ and 10.2 and 22.9 mJ m⁻² for calcite⁵⁰. It should be noted that the values quoted for calcite depend strongly on the thermal pre-treatment and state of hydration of the calcite surface⁵⁰⁻⁵³. The

values used here correspond to water-saturated calcite since this is most likely to correspond to the calcite powders in the packed column flooding experiments. If the surface energies of two components x and y against air are known, the x-y interfacial energy can be calculated using⁴⁹:

$$\gamma_{x-y} = \gamma_{x-air} + \gamma_{y-air} - 2\sqrt{\gamma_{x-air}^p \gamma_{y-air}^p} - 2\sqrt{\gamma_{x-air}^d \gamma_{y-air}^d} \quad (3)$$

Using equation 3 and the surface energy components noted above, the three interfacial tensions in the absence of surfactant were calculated; $\gamma_{decane-water,0} = 50.5$, $\gamma_{calcite-water,0} = 15.3$ and $\gamma_{decane-calcite,0} = 10.2$ mN m⁻¹. From the three interfacial tensions, the water-calcite-decane contact angle θ (through the water) is given by Young's equation.

$$\cos \theta = \frac{\gamma_{calcite-decane} - \gamma_{calcite-water}}{\gamma_{water-decane}} \quad (4)$$

which yields a value of 96° for pure water, slightly lower than but comparable with the value of 120±10° measured for water containing Na₂CO₃ and NaCl. In order to calculate the variation of contact angle with surfactant concentration, the variation of the three interfacial tensions with surfactant concentration must be estimated. The decane-water tension as a function of AOT concentration is measured directly. It is known that AOT monomer does not partition to a measurable extent from aqueous solution containing NaCl to alkane solvents³⁶ and hence it is assumed here that $\gamma_{decane-calcite}$ remains equal to its value in the absence of AOT $\gamma_{decane-calcite,0}$ for all AOT concentrations. For the calcite-water interface, the tension as a function of AOT concentration is obtained by integration of the measured adsorption isotherm according to the Gibbs adsorption equation⁵⁴.

$$\gamma_{calcite-water} = \gamma_{calcite-water,0} - kT \int_0^C \frac{\Gamma(C)}{C} dC \quad (5)$$

where k is Boltzmann's constant, T is the absolute temperature and $\Gamma(C)$ is the surface concentration of adsorbed AOT as a function of the AOT concentration C. Figure 4 shows the three interfacial tensions estimated as described above and the corresponding variation of derived contact angle θ with AOT concentration and comparison with the measured angles. Despite the large uncertainty in the surface energy components of calcite, it can be seen that the calculated plot correctly predicts the

slight increase in angle as [AOT] approaches the $c_{\mu c}$ and the sharp decrease in θ at $[AOT] \approx c_{\mu c}$. For $[AOT] > c_{\mu c}$, the calculations predict that $\theta = 0^\circ$ whereas the measured values are in the range $40-15^\circ$. A possible reason for this discrepancy could be that the assumption of no AOT adsorption from decane to the decane-calcite interface (based on the observed lack of partitioning of AOT from aqueous NaCl solution to alkanes³⁶) may not be valid in the presence of calcium carbonate. Leaching of calcium ions from the calcite might produce $Ca(AOT)_2$ species that may partition into decane and adsorb at the decane-calcite interface. Such partitioning and adsorption could potentially decrease $\gamma_{\text{decane-calcite}}$ and increase θ at high [AOT]. Additional considerations of how surfactants can affect contact angles relevant to EOR, e.g. solid surface roughness and surfactant mixture effects are described in refs. 55-56.

Decane removal from a calcite packed column by aqueous surfactant solutions.

As described in the experimental section, most decane removal experiments were made by pumping aqueous solution at a fixed flow rate of $5 \mu\text{l min}^{-1}$ into the packed column. This volumetric flow rate corresponds to an average linear velocity of the pumped fluid through the column u (equal to $Q/\phi_{\text{pore}}A$) of approximately $2.5 \times 10^{-6} \text{ m s}^{-1}$ (equal to 0.7 feet per day), similar to actual field conditions⁴. The interplay of pumped fluid velocity (determining viscous forces) and pore-scale capillary effects on the oil mobilisation is normally discussed in terms of the capillary number Ca which is the ratio of viscous and capillary forces acting on a fluid element. It is expected that, when $Ca < 1$, flow is dominated by capillary effects and oil is trapped in the porous network. Oil is released when $Ca > 1$ and the flow is dominated by viscous effects. However, as discussed in ref. 57, the correct estimation of Ca for multiphase flow in a porous network has been a long-standing controversy because of the difficulty of estimating the viscous and capillary forces over identical and correct length scales. In the EOR field, Ca is commonly defined as $u\mu/\gamma_{\text{oil-water}}$, for which the velocity u is an average value over a macroscopic length scale. According to this definition of Ca , oil mobilisation under typical field conditions occurs for Ca values greater than about 10^{-5} to 10^{-7} ,

much less than the expected threshold value of Ca equal to unity. In addition, the threshold value of Ca depends on the morphology of the porous network, its wettability and its oil and water content in ways which are not completely understood. Hence, although Ca provides some useful correlations to interpret the variation of oil recovery with fluid velocity, viscosity and oil-water tension, there are severe difficulties in using it for quantitative predictions.

Qualitatively, it is expected that the amount of oil recovery (after injection of >1 pore volume) should be independent of pumped fluid flow rate when Ca is very low and to increase with flow rate at high values of Ca. As seen in Figure S5, the oil recovery using pure water is independent of flow rate below 0.005 ml min⁻¹. This flow rate corresponds to a threshold value of Ca of approximately 6×10^{-9} ($\gamma_{\text{oil-water}}$ is 42.5 mN m⁻¹). When surfactant solution is used, $\gamma_{\text{oil-water}}$ is 0.0078 mN m⁻¹, giving Ca values in the much higher range of 5×10^{-6} to 3×10^{-3} and the plot shows no flow rate independent region between 0.001 and 0.5 ml min⁻¹. Overall, it can be seen that for a constant imposed flow rate of 0.005 ml min⁻¹, systems with low AOT concentrations (< approx. $c_{\mu c}/2$) lie within the low Ca regime in which oil trapping is expected. Systems with AOT concentrations equal to the $c_{\mu c}$ or higher lie within the high Ca regime for which oil drop break-off and mobilisation is expected.

When surfactant solution is pumped into the packed column, the concentration of non-adsorbed surfactant present in the aqueous solution $[\text{surf}]_{\text{non-adsorbed}}$ is less than the initial concentration present in the pumped solution prior to entry of the column $[\text{surf}]_{\text{init}}$ due to depletion by adsorption at the calcite-water and the decane-water interfaces. When oil recovery is high, the depletion due to adsorption at the trapped decane-water interfaces is likely to be small and is assumed negligible here. Consideration of the surfactant mass balance in a system comprising the packed column plus n pore volumes of aqueous solution leads to the following relationship between $[\text{surf}]_{\text{init}}$ and $[\text{surf}]_{\text{non-adsorbed}}$.

$$[surf]_{init} = \frac{\{n\phi_{pore}[surf]_{non-adsorbed} + (1-\phi_{pore}) \cdot f \cdot A_{particle} \rho \cdot \Gamma / N_{Av}\}}{n\phi_{pore}} \quad (6)$$

where n is the number of pore volumes pumped through the column, $A_{particle}$ is the surface area per mass of packed particles, ρ is the particle density and f is the fraction of the particle surface area which is accessible to the aqueous solution. The fraction f is less than unity since some of the particle surface area is covered with the decane trapped in the column, thereby rendering parts of the particle surface area not accessible to the aqueous solution. The relationship between $[surf]_{non-adsorbed}$ and adsorbed surface concentration Γ is given by the adsorption isotherm (equation 1), $A_{particle}$ and ϕ_{pore} are separately measured (Table 1), the calcite density is 2.71 g cm^{-3} and so the only unknown parameter is f . The model described below enables the estimation of f which depends on the fraction of oil remaining in the column. For the range of % oil recovery values measured here, f is estimated to be in the range 0.3 – 0.6. In order to simplify the calculations, a mean value of $f = 0.4$ was used to convert the values of $[surf]_{init}$ to $[surf]_{non-adsorbed}$ on the plots of % oil recovery versus surfactant concentration. This scale transformation enables the values of % oil recovery to be linked directly with the corresponding values of interfacial tensions, contact angles and critical aggregation concentrations. In addition, the difference ($[surf]_{init} - [surf]_{non-adsorbed}$) provides a measure of the “wasted” surfactant which is retained by the packed column and is therefore likely to provide an important input into the assessment of the economic viability of the oil recovery.

Modelling how % oil recovery depends on surfactant concentration

As described above, we have measured the % oil recovery under low flow rate conditions such that capillary forces dominate over viscous forces, at least for systems in the absence of surfactant. The % oil recovery has been measured at surfactant concentrations ranging from below to above the critical aggregation concentration. For surfactant concentrations below the critical aggregation concentration, the surfactant potentially affects the % oil recovery only because of the changes in the contact angle and the value of the oil-water tension. Above the critical aggregation concentration (when the concentration of non-adsorbed, non-aggregated surfactant, contact angle and

oil-water tension all remain constant), the surfactant aggregates present can additionally remove oil by solubilisation. As detailed below, both these mechanisms are invoked to model the measured plots of %oil recovery as a function of surfactant concentration.

We first consider how the % oil recovery is affected by contact angle θ and oil-water tension γ . In order to (greatly) simplify the calculations, we take the packed particle bed to consist of monodisperse spheres packed in a cubic arrangement as shown in Figure 5. This type of cubic packing was selected because the volume fraction of interstitial space (denoted as ϕ_{pore} here) is equal to $(1 - \pi/6) = 0.48$ and is close to the value of $\phi_{\text{pore}} = 0.45$ measured for the randomly packed FC10 calcium carbonate particles used here. We postulate that, following flooding by aqueous surfactant solution, the oil remaining in the particle packed column is trapped in the form of liquid bridges between contacting particles⁵⁸⁻⁶⁰, as shown in Figure 5. For the calculations, the profile of the liquid bridge is approximated as a circular arc. Using EXCEL, we calculate the profiles, volumes and surface areas for a set of liquid bridges which all have a constant value of contact angle θ but different values of the parameter h defined in Figure 5. For each bridge of different h value, the known geometry of the bridge's curved oil-water interface and the value of the oil-water tension enables the calculation of the Laplace pressure difference across the oil-water interface ΔP_{bridge} . A positive value of ΔP_{bridge} indicates that the pressure inside the bridge is higher than outside the bridge. We next consider what factors determine the size of the oil bridge which is stranded as aqueous surfactant solution is pumped through the initially oil-filled packed bed. We assume that the water flows through the particle interstices indicated by the dashed circle in Figure 5. The size of this flow channel depends on the size of the residual oil liquid bridges. We estimate the average, effective radius of these flow channels (denoted as r_{chan}) as the radius of the circle which has an area equal to the area of the particle interstice minus the areas of the four liquid bridges in contact with it. We also assume that r_{chan} cannot exceed the radius of the circle circumscribed by the particles ($= r_{\text{chan,max}}$). Thus, by setting the value of h for the liquid bridges, we are then able to calculate r_{chan} for a

set value of liquid bridge size. In order to achieve flow through r_{chan} , the driving pressure must exceed the maximum Laplace pressure difference which occurs when a hemi-spherical “bulge” of aqueous phase into the oil-filled interstice occurs. This maximum Laplace pressure $\Delta P_{\text{chan}} = 2\gamma/r_{\text{chan}}$ and is also known as the capillary entry pressure. For fixed contact angle θ and oil-water tension γ , the system can “choose” whether to bulge and breakthrough through small pores and leave large liquid bridges (thereby giving a low % oil recovery) or to bulge and create large flow channels and leave small liquid bridges. We postulate here that the size of the trapped liquid bridges and corresponding value of the flow channel size r_{chan} is determined by the condition that $\Delta P_{\text{bridge}} = \Delta P_{\text{chan}}$ (for $r_{\text{chan}} < r_{\text{chan,max}}$) or that $r_{\text{chan}} = r_{\text{chan,max}}$. The resulting estimation of %oil recovery is found to depend only on the contact angle θ and to be independent of the decane-water interfacial tension.

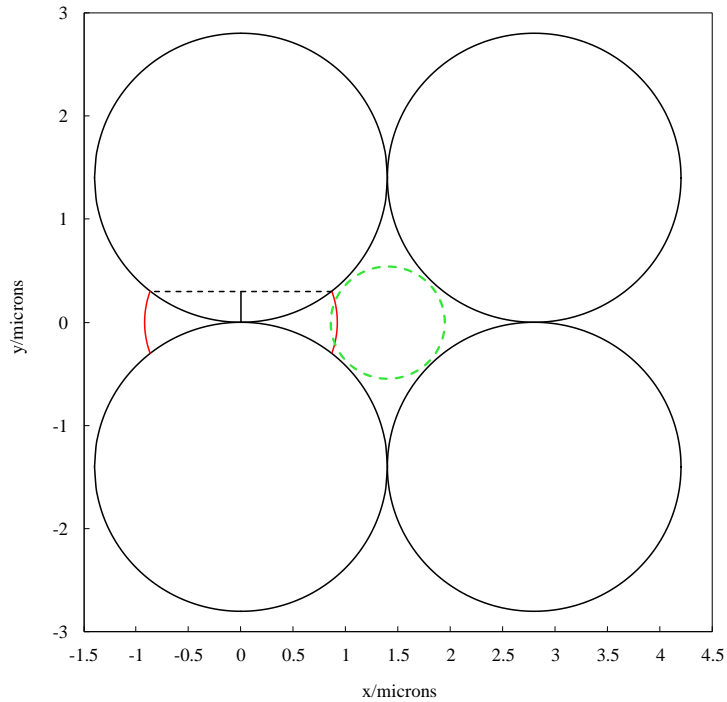


Figure 5. Cubic packing of calcite spheres showing the cross sectional profile of a liquid oil bridge (red), the distance h (vertical solid black line) and the circular profile of a water phase flow channel (green dashed line). Note that only a single oil liquid bridge is shown here; each particle-particle contact point is assumed to have an identical liquid bridge. The configuration shown here is calculated for calcite-water-oil contact angle θ (measured through the water) equal to 107° , particle radius = $1.4 \mu\text{m}$ and $h = 0.3 \mu\text{m}$.

The theory outlined above enables the estimation of % oil recovery due to the effect of the added surfactant on the contact angle θ . For surfactant concentrations in excess of the $c_{\mu c}$, two additional factors arise. Firstly, the additional surfactant is present in the form of aggregates which can also remove trapped oil by solubilisation. To estimate this contribution, we assume that each mole of aggregated surfactant solubilises R_{sol} moles of decane, where R_{sol} is the equilibrium solubilisation molar ratio equal to $[\text{solubilised decane}]/([\text{AOT}] - c_{\mu c})$. Based on this assumption, the %oil recovered by solubilisation using n pore volumes of aqueous phase is given by

$$\%oil_{sol} = n MV_{decane} R_{sol} ([AOT] - c_{\mu c}) \quad (7)$$

where MV_{decane} is the molar volume of decane. The total %oil recovery is equal to the sum of the contributions from the contact angle effect and from the solubilisation. Secondly, as discussed above, when the surfactant concentration is increased to $>c_{\mu c}$, the oil-water tension reaches a very low value and the system moves from the low to the high capillary number regime. In this high Ca regime, viscous forces dominate over capillary forces which leads to the breakup and mobilisation of trapped oil. This process is similar to emulsification in which the newly formed emulsion drops require adsorption of surfactant to be stabilised. In order that the oil-water tension does not increase, only surfactant in excess of the $c_{\mu c}$ is likely to adsorb to the newly formed emulsion drops. Hence, the amount of oil mobilisation by breakup and mobilisation (emulsification) is likely to be proportional to $([AOT] - c_{\mu c})$. We assume here that R_{em} moles of decane is emulsified per mole of aggregated AOT in excess of the $c_{\mu c}$. The %oil recovered by solubilisation plus emulsification using n pore volumes of aqueous phase is then given by

$$\%oil_{sol+em} = n MV_{decane} (R_{sol} + R_{em}) ([AOT] - c_{\mu c}) \quad (8)$$

Figure 6 compares the measured variation of %oil recovery as a function of the non-adsorbed AOT concentration for systems containing 75 mM NaCl and 10 mM Na_2CO_3 with the model calculations. With increasing AOT concentration, the %oil recovery increases slightly up to the $c_{\mu c}$ when it sharply decreases before increasing again. From the model calculations, the oil recovery resulting from changes in contact angle increases slightly up to the $c_{\mu c}$ and decreases sharply at the $c_{\mu c}$ when θ decreases strongly. The increase in oil recovery above the $c_{\mu c}$ is reasonably well represented by equation 8 with a value of $(R_{sol} + R_{em})$ equal to 600 moles of decane per mole of aggregated AOT. The maximum equilibrium solubilisation ratio of decane by AOT under these conditions (R_{sol}) is approximately 10 (by extrapolation of the data from ref. 37). Hence, for the system of Figure 6 with an ultralow value of the post- $c_{\mu c}$ oil-water interfacial tension equal to 0.0079 mN m^{-1} , the bulk of the post- $c_{\mu c}$ increase in oil recovery occurs by breakup and mobilisation

(emulsification) of the trapped oil as a result of the high capillary number. We note that the uncertainties in the %oil recovery values for $[AOT] > c_{\mu c}$ are larger than the uncertainty of $\pm 2\%$ estimated from repeatability measurements of the mass of packed column (see Experimental). This greater irreproducibility observed above the $c_{\mu c}$ may be due to slight variations in the calcite particle packing from run to run having a large effect on the %oil recovery due to solubilisation and emulsification (but not on the oil recovery resulting only from contact angle changes for $[AOT] < c_{\mu c}$).

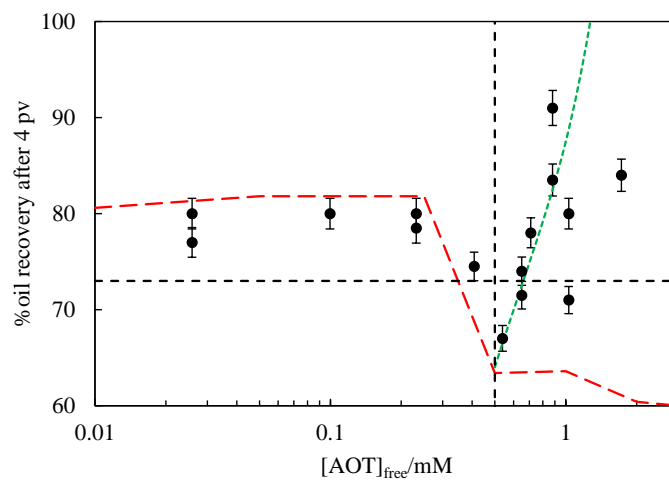


Figure 6. Variation of %oil recovered after 4 pore volumes as a function of the non-adsorbed (free) AOT concentration for solutions containing 75 mM NaCl and 10 mM Na₂CO₃. The vertical black dashed line shows the $c_{\mu c}$ and the horizontal black dashed line indicates the %oil recovered in the absence of AOT. The red dashed line shows the %oil recovered from the contact angle alone mechanism, and the green dotted line the %oil recovered from the contact angle and the solubilisation/emulsification mechanisms combined, both calculated using the model described in the text.

We interpret the %oil recovery after 4 pore volumes as resulting from surfactant-induced contact angle changes plus solubilisation/emulsification for AOT concentrations above the $c_{\mu c}$. For

systems containing AOT concentration $\leq c_{\mu c}$, the %oil recovery resulting from contact angle changes should be complete following the injection of approximately 1 pore volume whereas the contribution from solubilisation and emulsification (for AOT concentrations $> c_{\mu c}$) should continue to increase with the number of pore volumes injected. The upper plot of Figure 7 compares plots of %oil recovery versus pores volumes injected for systems above and below the $c_{\mu c}$. Below the $c_{\mu c}$, when oil recovery occurs only by contact angle change, the oil recovered remains constant after 1 pore volume. Above the $c_{\mu c}$, where oil recovery occurs by both contact angle change and solubilisation plus emulsification, the recovery continues to rise after 1 pore volume. The lower plot of Figure 7 shows the difference in oil recovery between 1 and 4 pore volumes as a function of the non-adsorbed AOT concentration. Consistent with the model proposed here, the difference in recovery is only significant for AOT concentrations in excess of the $c_{\mu c}$.

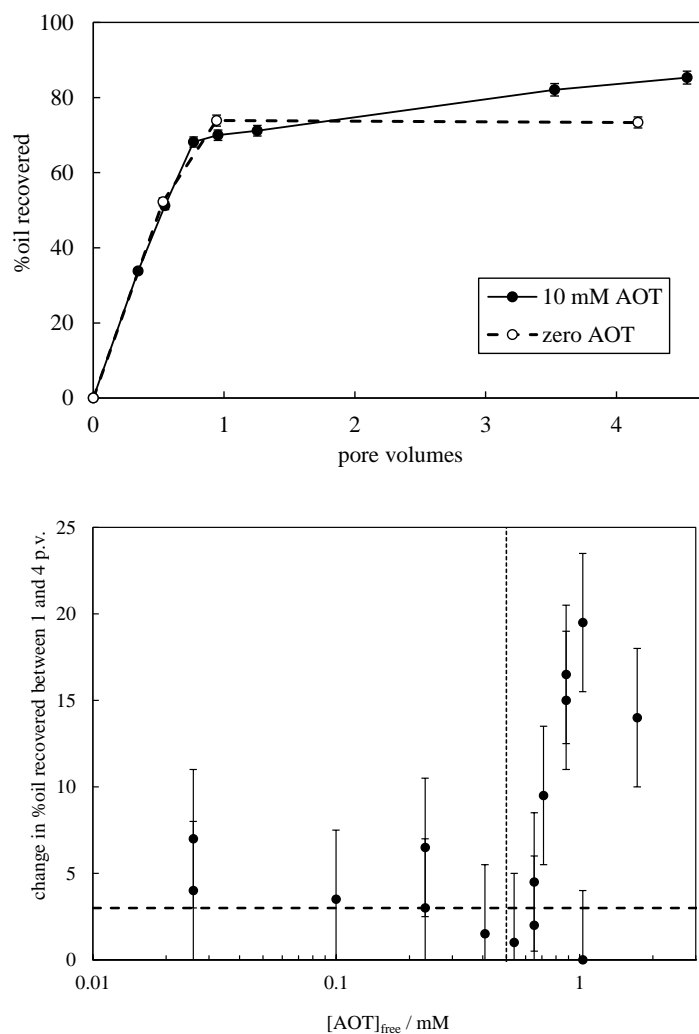


Figure 7. Upper plot: variation of %oil recovery with number of pore volumes pumped for $0.005 \text{ ml min}^{-1}$ of aqueous solutions containing 75 mM NaCl and $10 \text{ mM Na}_2\text{CO}_3$ into an FC10 packed column with pore volume fraction 0.45 initially containing decane. Plots for 10 mM AOT and zero AOT are compared. Lower plot: variation of the change in %oil recovery between 1 and 4 pore volumes versus $[\text{AOT}]_{\text{free}}$ for AOT solutions containing 75 mM NaCl and $10 \text{ mM Na}_2\text{CO}_3$ pumped into an FC10 packed column initially containing decane.

From Figure 6, the oil recovery from solubilisation/emulsification after 4 pore volumes is estimated to be 600 moles of decane per mol of aggregated AOT in the 75 mM NaCl system for which the oil-water tension is ultralow (0.0078 mN m^{-1}). Figure S6 shows the oil recovery plot for

systems containing zero NaCl for which the post-c_{uc} oil-water tension is much higher (0.33 mN m⁻¹). In this case, the value of (R_{sol} + R_{em}) is estimated to be approximately 60; ten-fold lower than the ultralow, minimum tension system.

Finally, we note an additional factor which may affect the % oil recovery for [AOT] > c_{uc}. As noted previously, the AOT solutions used here give microemulsion phases in equilibrated mixtures with decane. However, the solutions injected here are not pre-equilibrated with decane. Below the critical aggregation concentration (cac, similar in magnitude to the c_{uc}), they are single-phase solutions containing AOT monomers. Above the cac, they consist of slightly turbid dispersions of lamellar phase, probably in the form of multilamellar, “onion-like” vesicles³⁸⁻³⁹ in equilibrium with AOT monomers. On equilibration with decane, these mixtures solubilise decane to form either oil-in-water or bicontinuous microemulsions¹⁹. When these dispersions are injected into the packed column, the dispersed fragments of lamellar phase are expected to increase the resistance to flow through the column. Consistent with this idea, the plot of measured pressure drop versus volume of liquid pumped (Figure 8) rises to a maximum value which is considerably larger than the pressure drop required to achieve the imposed flow rate and the estimated capillary pressure. The pressure drop decreases progressively between 1 and 4 pore volumes rather than reaching a plateau value as seen for other systems in Figure S4a-c. The increased driving pressure from the flow restriction may act to further increase the removal of trapped oil.

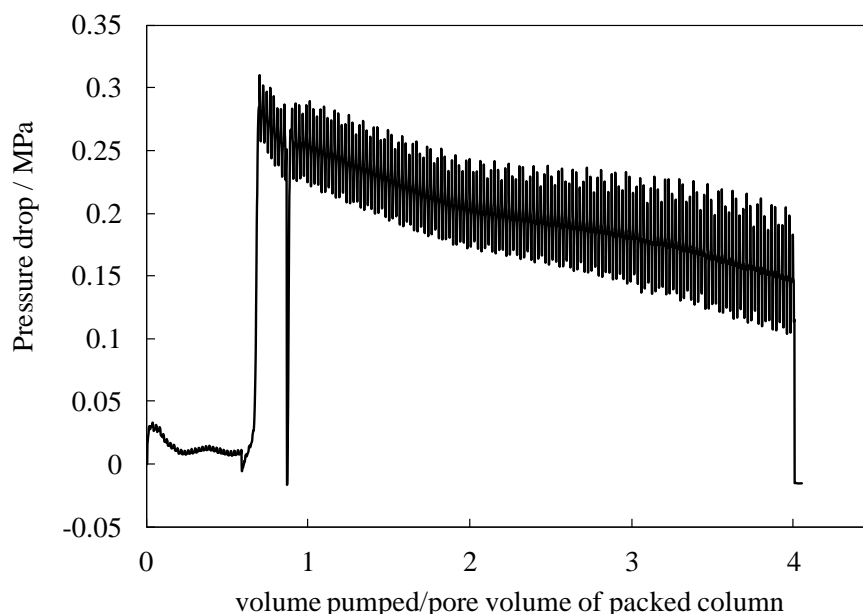


Figure 8. Variation of pressure drop (between pressure sensor 2 and column exit) with volume of water containing 7 mM AOT and 10 mM Na₂CO₃, pumped at 0.005 ml min⁻¹ into an FC10 packed column with pore volume fraction 0.45 initially containing decane. (Oil-water tension = 0.33 mN m⁻¹, contact angle through water = 0°, estimated capillary pressure ΔP_{cap} (calculated as either $2\gamma/r_{\text{pore}}$ or $2\gamma/r_{\text{chan}}$) = -0.0041 to -0.0011 MPa and the estimated pressure drop required for liquid flow ΔP_{flow} = 0.044 MPa.)

Conclusions

The main novel aspect of this study lies in the full and systematic determination of the surface and colloid chemistry system properties and their use to explicitly model the oil recovery. We have shown how the variation of contact angle with surfactant concentration is related to the measured tensions and adsorption isotherms. Knowledge of the adsorption isotherm enables the estimation of the concentration of non-adsorbed surfactant in the packed column experiments which, in turn, allows detailed analysis of the %oil recovery variation with surfactant concentration in terms of the measured contact angles and the $c_{\mu c}$. We show that, for surfactant concentrations $< c_{\mu c}$, the %oil recovery is determined by the contact angle. Above the $c_{\mu c}$, additional oil is recovered by a solubilisation plus emulsification mechanism.

Acknowledgements

We thank the University of Hull and Schlumberger Gould Research Laboratory for providing PhD Studentship funding.

Supporting Information Available: This material is available free of charge via the Internet at <http://pubs.acs.org>. **Figures S1-S6** show SEM images of the calcium carbonate powders, permeability measurements of the packed columns, size distributions of the calcite powders, example plots of pressure drop versus pumped volume and variation of %oil recovery with flow rate and other variables.

References

1. Babadagli, T. Development of mature oil fields – a review. *J. Petroleum Sci. Eng.*, **2007**, *57*, 221-246.
2. Sheng, J.J. Modern chemical enhanced oil recovery: theory and practice. **2011**, Elsevier, Amsterdam.
3. Warren, J.E.; Calhoun, J.C. A study of waterflood efficiency in oil-wet systems. *Petroleum Trans.*, **1955**, *204*, 22-29.
4. Morrow, N.R.; Mason, G. Recovery of oil by spontaneous imbibitions. *Curr. Opin. Colloid Interface Sci.*, **2001**, *6*, 321-337.
5. Babadagli, T. Evaluation of the critical parameters in oil recovery from fractured chalks by surfactant injection. *J. Petroleum Sci. Eng.*, **2006**, *54*, 43-54.
6. Hirasaki, G.J.; Miller, C.A.; Puerto, M. Recent advances in surfactant EOR. *Soc. Petroleum Eng. J.*, **2011**, *16*, 889-901.
7. Jeirani, Z.; Mohamed Jan, B.; Si Ali, B.; See, C.H.; Saphanuchart, W. Pre-prepared microemulsion flooding in enhanced oil recovery: a review. *Petroleum Sci. Technol.*, **2014**, *32*, 180-193.
8. Jeirani, Z.; Mohamed Jan, B.; Si Ali, B.; See, C.H.; Saphanuchart, W. In situ prepared microemulsion-polymer flooding in enhanced oil recovery: a review. *Petroleum Sci. Technol.*, **2014**, *32*, 240-251.
9. Sheng, J.L. A comprehensive review of alkaline-surfactant-polymer (ASP) flooding. *Asia-Pac. J. Chem. Eng.*, **2014**, *9*, 471-489.
10. Standnes, D.C.; Austad, T. Wettability alteration in chalk. 2. Mechanism for wettability alteration from oil-wet to water-wet using surfactants. *J. Petroleum Sci. Eng.*, **2000**, *28*, 123-143.

11. Standnes, D.C.; Austad, T. Wettability alteration in carbonates. Interaction between cationic surfactant and carboxylates as a key factor in wettability alteration from oil-wet to water-wet conditions. *Colloids Surfaces A*, **2003**, *216*, 243-259.
12. Wu, Y.; Shuler, P.J.; Blanco, M.; Tang, Y.; Goddard, W.A. An experimental study of wetting behaviour and surfactant EOR in carbonates with model compounds. *Soc. Petroleum Eng. J.*, **2008**, March, 26-34.
13. Yefei, W.; Huaimin, X.; Weizhao, Y.; Baojun, B.; Xinwang, S.; Jichao, Z. Surfactant induced reservoir wettability alteration: recent theoretical and experimental advances in enhanced oil recovery. *Petroleum Sci.*, **2011**, *8*, 463-476.
14. Jarrahan, Kh.; Seiedi, O.; Sheykhan, M.; Sefti, M.V.; Ayatollahi, Sh. Wettability alteration of carbonate rocks by surfactant: a mechanistic study. *Colloids Surfaces A*, **2012**, *410*, 1-10.
15. Stohr, M.; Roth, K.; Jahne, B. Measurement of 3D pore-scale flow in index-matched porous media. *Exp. Fluids*, **2003**, *35*, 159-166.
16. Jamaloei, B.Y.; Asghari, K.; Kharrat, R. Pore-scale flow characterization of low-interfacial tension flow through mixed-wet porous media with different pore geometries. *Exp. Thermal Fluid Sci.*, **2011**, *35*, 253-264.
17. Karadimitriou, N.K.; Hassanizadeh, S.M. A review of micromodels and their use in two-phase flow studies. *Vadose Zone J.*, **2012**, *11*, DOI: 10.2136/vzj2011.0072
18. Krummel, A.T.; Datta, S.S.; Munstr, S.; Weitz, D.A. Visualizing multiphase flow and trapped fluid configurations in a model three-dimensional porous medium. *AIChE J.*, **2013**, *59*, 1022-1029.
19. Howe, A.M.; Clarke, A.; Whalan, C.; Hawkes, L.; Mitchell, J.; Staniland, J. Visualising surfactant enhanced oil recovery, *Colloids Surf. A: Physicochem. Eng. Aspects*, **2014**, <http://dx.doi.org/10.1016/j.colsurfa.2014.08.032>

20. Buckley, S.E.; Leverett, M.C. Mechanism of fluid displacement in sands. *Trans. Amer. Inst. Mining & Metallurg. Eng.*, **1942**, *146*, 107-116.
21. Chatzis, I.; Morrow, N.R., Correlation of capillary number relationships for sandstone. *Soc. Petroleum Eng. J.*, **1984**, *24*, 555-562.
22. Hammond, P.S. Unsal, E. Spontaneous and forced imbibition of aqueous wettability altering surfactant solution in an initially oil-wet capillary. *Langmuir*, **2009**, *25*, 12591-12603.
23. Hammond, P.S. Unsal, E. Forced and spontaneous imbibitions of surfactant solution in an oil-wet capillary: the effects of surfactant diffusion ahead of the advancing meniscus. *Langmuir*, **2010**, *26*, 6206-6221.
24. Hammond, P.S. Unsal, E. Spontaneous imbibition of surfactant solution in an oil-wet capillary: wettability restoration by surfactant-contaminant complexation. *Langmuir*, **2011**, *27*, 4412-4429.
25. Sheng, J.L. Comparison of the effects of wettability alteration and IFT reduction on oil recovery in carbonate reservoirs. *Asia-Pacific J. Chem. Eng.*, **2013**, *8*, 154-161.
26. Blunt, M.J.; Bijeljic, B.; Dong, H.; Gharbi, O.; Iglauer, S.; Mostaghimi, P.; Paluszny, A.; Pentland, C. Pore-scale imaging and modelling. *Adv. Water Res.*, **2013**, *51*, 197-216.
27. Wammes, W.J.A.; Mechielsen, S.J.; Westerterp, K.R. The influence of pressure on the liquid hold-up in a concurrent gas-liquid trickle-bed reactor operating a low gas velocities. *Chem. Eng. Sci.*, **1991**, *46*, 409-417.
28. Zeinal Heris, S.; Hamad Mosavian, M.T.; White, E.T. Capillary holdup between vertical spheres. *Brazilian J. Chem. Eng.*, **2009**, *26*, 695-704.
29. Schwidder, S.; Schnitzlein, K. Predicting the static liquid holdup for cylindrical packings of spheres in terms of the local structure of the packed bed. *Chem. Eng. Sci.*, **2010**, *65*, 6181-6189.

30. Barrett, E.P.; Joyner, L.G.; Halenda, P.P. The determination of pore volume and area distributions in porous substances. I. Computations from nitrogen isotherms. *J. Amer. Chem. Soc.*, **1951**, *73*, 373-380.
31. Reid, V.W.; Longman, G.F.; Heinerth, E. Determination of anionic-active detergents by two-phase titration. *Tenside*, **1967**, *4*, 292-304.
32. Reed, R.L.; Healy, R.N. Contact angles for equilibrated microemulsion systems. *Soc. Petroleum Eng. J.*, **1984**, *27*, 342-350.
33. Salager, J-L.; Forgiarini, A.M.; Bullon, J. How to attain ultralow interfacial tension and three-phase behaviour with surfactant formulation for enhanced oil recovery: a review. Part 1. Optimum formulations for simple surfactant-oil-water ternary systems. *J. Surfact. Deterg.*, **2013**, *16*, 449-472.
34. Salager, J-L.; Forgiarini, A.M.; Marquez, L.; Manchego, L.; Bullon, J. How to attain ultralow interfacial tension and three-phase behaviour with surfactant formulation for enhanced oil recovery: a review. Part 2. Performance improvement trends from Winsor's premise to currently proposed inter- and intra-molecular mixtures. *J. Surfact. Deterg.*, **2013**, *16*, 631-663.
35. Fraaije, J.G.E.M.; Tandon, K.; Jain, S.; Handgraaf, J-W.; Buijse, M. Method of moments for computational microemulsion analysis and prediction in tertiary oil recovery. *Langmuir*, **2013**, *29*, 2136-2151.
36. Aveyard, R.; Binks, B.P.; Clark, S.; Mead, J. Interfacial tension minima in oil-water-surfactant systems Behaviour of alkane-aqueous NaCl systems containing Aerosol OT. *J. Chem. Soc. Faraday Trans. 1*, **1986**, *82*, 125-142.
37. Fletcher, P.D.I. Characterisation of Aerosol OT-stabilised oil-in-water microemulsions using a time-resolved fluorescence method. *J. Chem. Soc. Faraday Trans. 1*, **1987**, *83*, 1493-1506.

38. Skouri, M.; Marignan, J.; May, R. X-ray and neutron-scattering study of the lamellar and L₃ phases of the system aerosol-OT-water: effect of NaCl and decane. *Colloid & Polymer Sci.*, **1991**, *269*, 929-937.
39. Balinov, B.; Olsson, U.; Soderman, O. Structural similarities between the L₃ and bicontinuous cubic phases in the AOT-brine system. *J. Phys. Chem.*, **1991**, *95*, 5931-5936.
40. Somasundaran, P.; Agar, G.E. The zero point of charge of calcite. *J. Colloid Interface Sci.*, **1967**, *24*, 433-440.
41. Moulin, P.; Roques, H. Zeta potential measurement of calcium carbonate. *J. Colloid Interface Sci.*, **2003**, *261*, 115-126.
42. Eriksson, R.; Merta, J.; Rosenholm, J.B. The calcite/water interface I. Surface charge in indifferent electrolyte media and the influence of low-molecular-weight polyelectrolyte. *J. Colloid Interface Sci.*, **2007**, *313*, 184-193.
43. Eriksson, R.; Merta, J.; Rosenholm, J.B. The calcite/water interface II. Effect of added lattice ions on the charge properties and adsorption of sodium polyacrylate. *J. Colloid Interface Sci.*, **2008**, *326*, 396-402.
44. Sondi, I.; Biscan, J.; Vdovic, N.; Skapin, S.D. The electrokinetic properties of carbonates in aqueous media revisited. *Colloids & Surfaces A*, **2009**, *342*, 84-91.
45. Heberling, F.; Trainor, T.P.; Lutzenkirchen, J.; Eng, P.; Denecke, M.A. Bosbach, D. Structure and reactivity of the calcite-water interface. *J. Colloid Interface Sci.*, **2011**, *354*, 843-857.
46. Brunauer, S.; Love, K.S.; Keenan, R.G. Adsorption of nitrogen and the mechanism of ammonia decomposition over iron catalysts. *J. Amer. Chem. Soc.*, **1942**, *64*, 751-758.
47. Foo, K.Y.; Hameed, B.H. Insights into the modelling of adsorption isotherm systems. *Chem. Eng. J.*, **2010**, *156*, 2-10.

48. Stocker, I.N.; Miller, K.L.; Welbourn, R.J.L.; Clarke, S.M.; Collins, I.R.; Kinane, C.; Gutfreund, P. Adsorption of Aerosol-OT at the calcite/water interface – Comparison of the sodium and calcium salts. *J. Colloid Interface Sci.*, **2014**, *418*, 140-146.
49. van Oss, C.J. *Interfacial forces in aqueous media*, New York: Marcel Dekker, **1994**.
50. Schoff, C.K. Wettability phenomena and coatings. Chap. 14, pp. 375-395 in Schrader, M.E. Loeb, G. (Eds.) *Modern approach to wettability: theory and applications*. Plenum Press, New York, **1992**.
51. Okayama, T.; Keller, D.S.; Luner, P. The wetting of calcite surfaces. *J. Adhesion*, **1997**, *63*, 231-252.
52. Keller, D.S.; Luner, P. Surface energetic of calcium carbonates using inverse gas chromatography. *Colloids & Surfaces A*, **2000**, *161*, 401-415.
53. Arsalan, N.; Palayangoda, S.S.; Burnett, D.J., Buiting, J.J.; Nguyen, Q.P. Surface energy characterization of carbonate rocks. *Colloids & Surfaces A*, **2013**, *436*, 139-147.
54. Lucassen-Reynders, E.H. Contact angles and adsorption on solids. *J. Phys. Chem.*, **1963**, *67*, 969-972.
55. Morrow, N.R. The effects of surface roughness on contact angle with special reference to petroleum recovery. *J. Can. Petroleum Technol.*, **1975**, *14*, 42-53.
56. Somasundaram, P.; Zhang, L. Adsorption of surfactants on minerals for wettability control in improved oil recovery processes. *J. Petroleum Sci. Eng.*, **2006**, *52*, 198-212.
57. Armstrong, R.T.; Georgiadis, A.; Ott, H.; Klemin, D.; Berg, S. Critical capillary number: desaturation studied with fast X-ray computed microtomography. *Geophys. Res. Lett.*, 2014, *41*, 55-60.
58. Haines, W.B. Studies in the physical properties of soils. II A note on the cohesion developed by capillary forces in an ideal soil. *J. Agric. Sci.*, **1925**, *15*, 529-535.

59. Fisher, R.A. On the capillary forces in an ideal soil; correction of formulae given by W.B. Haines. *J. Agric. Sci.*, **1926**, *16*, 492-505.
60. Kralchevsky, P.A.; Nagayama, K. Capillary bridges and capillary-bridge forces. In “Particles at fluid interfaces and membranes”, Elsevier, Amsterdam, **2001**, chap. 11, pp. 469-502.

Table of Contents Graphic

We measure and model how surfactant enhanced oil recovery varies with surfactant concentration.

